

Performance Evaluation of Single Stage Flash Evaporation Desalination Unit Integrated with a Parabolic Trough Solar Collector for Basrah City Climate, Iraq

M. Kareem Salim^{1,*}, Hussien S. Sultan², Falah A. Abood³

^{1,2,3} Department of Mechanical Engineering, College of Engineering, University of Basrah, Basrah, Iraq

¹ General Company for Ports of Iraq (GCPI), Department of Shipyard and Marine Industries, Basrah, Iraq

E-mail addresses: pgs.mohammed.kareem@uobasrah.edu.iq, hussien.sultan@uobasrah.edu.iq, falah.abood@uobasrah.edu.iq

Received: 11 December 2023; Revised: 5 February 2024; Accepted: 14 February 2024; Published: 15 February 2024

Abstract

Solar energy is the most suitable among all renewable energy options for competing with fossil fuels in desalination due to its ability to utilize both heat and power for the process. In this study, the Parabolic Trough Solar Collector (PTSC) for powering a Single Stage Flash (SSF) desalination unit was proposed for Basrah city climate, Iraq. The desalination system comprises two directly coupled sub-systems: the PTSC and the SSF desalination unit. The preheated feed brine water coming from condenser was used as a Heat Transfer Fluid (HTF) for PTSC, which gets heated to a desired temperature referred to as the Top Brine Temperature (TBT). The numerical simulations were performed via EBSILON professional 16.02 (2022) software. The effects of TBT, mass flowrate of feed brine water to get the desired TBT, solar collector area, and vacuum pressure inside flash chamber on the performance of the desalination system was studied. A major finding of the current study can be summarized as follows: The collector efficiency is enhanced eventually as TBT increases. The maximum values of distillate water in June are around 5.5, 4.56, 3.69, 2.75 and 1.85 kg/h for 12.408, 10.434, 8.3472, 6.26, and 4.1736 m² collector area respectively, when TBT 107 °C and vacuum pressure 40 kPa. For 1.598 m² collector area, the total distillate in the 1st of June amounted to 7.9 kg, with an average production rate of around 0.7 kg/h. The solar SSF system's productivity per solar collector unit area at 20 kPa, 15 kPa, and 10 kPa vacuum pressures was 4.7 kg/day/m², 5.3 kg/day/m², and 6.25 kg/day/m², respectively. The average Performance Ratio (PR) values are determined to be 0.694, 0.577, and 0.491 for 10 kPa, 15 kPa, and 20 kPa, respectively. These results are very acceptable when compared with an existing literature.

Keywords: Parabolic trough solar collector, Single stage flash desalination unit, Top brine temperature, Vacuum pressure.

<https://doi.org/10.33971/bjes.24.1.11>

1. Introduction

Desalination technology has become essential for providing distillate water in many global regions. Conventional desalination methods heavily rely on fossil fuels, resulting in high costs and increased environmental pollution. To address these issues, employing renewable energy sources in desalination plants emerges as a favorable alternative, offering economic, environmental, and sustainable advantages. Solar energy, a widely acknowledged sustainable resource, can effectively convert seawater into freshwater. Among various desalination technologies, Multi Stage Flash (MSF) desalination stands out for its exceptional water production rate, and surpassing other options in terms of efficiency. Darwish et al. [1] explored the effects of multiple factors on flashing efficiency. The results revealed that elevating the brine inlet temperature, expanding the flashing range, lowering the brine level, and reducing the brine flow rate were all associated with improved flashing efficiency. The experimental study conducted by Farwati [2] showed that a 1 m² flat plate collector coupled with MSF distillation system operating at 80 °C could produce approximately 8.2 m³ of distilled water annually, while a 1 m² compound collector operating at 122 °C could generate approximately 13.2 m³ annually.

Joseph et al. [3] successfully attained a maximum distillate yield of 8.5 kg/day using 2 m² flat plate collector, an evaporator, a single-stage vacuum pump, and a condenser. Nafey et al. [4]. designed and tested a solar flat plate-powered water desalination unit employing a flash evaporation process. The study revealed that in summer, the system achieved a daily productivity between 4.2 and 7 kg/day/m², while in winter, the range was 1.04 to 1.45 kg/day/m². These outcomes were obtained under an average mass flow rate of 0.0183 kg/s. Maroo et al. [5] presented a flash desalination system powered by solar energy. This system utilizes gravity and atmospheric pressure to generate a vacuum. They found that the single-stage system produced 0.707 kg/h, while the two-stage system yielded 1.12 kg/h under identical initial conditions with a mass flow rate of 20 kg/h feed saline water. Reddy et al. [6] developed a transient model to analyze a multi-stage evacuated solar desalination system connected to a flat plate collector. The purpose was to determine the best design configuration and assess system performance. The researchers examined various design and operating parameters to predict the optimal output. The optimal design conditions produced a maximum yield of 28.04 kg/m²/day and a minimum of 13.33 kg/m²/day.

Al-Hamahmy et al. [7] presented a novel approach to improve the efficiency of MSF desalination system. Their method involves extracting the cooling brine and directly re-

injecting it into stages without passing through the brine heater. This innovative system resulted in a notable 7.23 % enhancement in Gain Output Ratio (GOR), accompanied by a 3.47 % reduction in power consumption and a 3.90 % decrease in total cost. Roy et al. [8] created a mathematical model for a Once-Through (OT-MSF) desalination system. Their research explored the influence of a TBT of up to 160 °C on the design and performance aspects of MSF systems. At this elevated TBT, the PR was anticipated to rise significantly by 41.5% to reach 14.64, with a minor 0.9 % increase in specific area, representing a relatively small impact. Alsehli et al. [9] presented a new design used an array of concentrating solar collectors and a pair of thermal storage tanks, each with enough capacity to supply a 20-stage OT-MSF with brine for one day. The results indicated an average distillate production of 2230 m³/day with a solar array area of 42552 m², which could be expressed as 53 kg/m²/day. Garg et al. [10] developed a mathematical model to assess an MSF desalination system incorporating brine recirculation. The study highlighted that a Direct Absorption Solar Collector (DASC) effectively functioned as a heat source for the MSF system, resulting in a notably high GOR ranging from 11 to 14, depending on operational conditions.

Darawsheh [11] conducted an experimental investigation on a combined system incorporating a flat plate solar collector and a two-stage flash desalination system. The results revealed that reducing atmospheric pressure by 20 % within a vacuum flash chamber resulted in a notable 53% enhancement in the distillation to evaporation ratio and a significant 35% reduction in specific energy consumption. Alsheekh et al. [12] an experimental and numerical investigation on the Atmospheric Water Generator (AWG) device was conducted during August and September of 2019, as well as in March of 2020 in Basrah city. Their results showed that the device achieved a maximum water production of 3.4 kg/day on all testing days. This occurred within a range of relative humidity from 45% to 95% and temperatures spanning from 17 °C to 45 °C. Jaber et al. [13] An experimental investigation was conducted on the performance of a double slope solar still integrated with or without a PTSC. Their results showed that the integration of a PTSC with phase change material in the double slope solar still improved productivity by 37.3% and 42%, respectively. Alsehli [14] introduced an experimental prototype of a three-stage flash system combined with a flat plate solar collector. The results indicated an average distillate production of 10.3 kg/m²/day at a TBT of around 70°C. An economic analysis of the solar MSF plant demonstrated a per-unit production cost of 0.015 \$/L.

Babaebazaz et al. [15] designed a compact two-stage flash desalination unit incorporating a vacuum pump and a solar Parabolic Dish Collector (PDC) with a conical cavity receiver. Their efforts resulted in a maximum productivity of 0.644 kg/h, utilizing a saline feedwater flow rate of 0.7 kg/min, and the MSF functioned under a 10 kPa vacuum pressure. Thakur et al. [16] conducted an experiment where they integrated a PTSC to preheat water supplied to a still basin. Additionally, they utilized activated carbon pellets as a highly porous energy storage material to enhance evaporation rates and water production. The economic analysis of the modified unit estimated the cost of producing clean water at 0.010 \$/L. Farhadi et al. [17] investigated the impact of TBT, the number of stages, and ambient temperature on the performance of an MSF system powered by waste heat from the Abadan refinery complex for steam desalination. Their findings indicated that

an increase in TBT led to a significant improvement in exergy efficiency, GOR, and distillate water production, with increases of 34%, 47%, and 47%, respectively. Thabit et al. [18] introduced an Excel model for designing and assessing the energy needs of a 16-stage MSF desalination process. To validate the model, they simulated the 16 stages using EBSILON software. Their findings indicated that a decrease of 5°C in seawater temperature would lead to a reduction in the MSF plant's water production by 1000-3000 m³/day.

In this paper, a proposed solar flash desalination system in Basrah city is simulated via EBSILON professional 16.02 (2022) software. The aim of the current study is to utilize the solar energy availability for Basrah city via a PTSC to completely drive the flash desalination system, and finding the possibility of applying the proposed system in Basrah city climate. Very rare studies, conducting an experimental or numerical study, have been discovered that focused on the utilization of a PTSC to power a flash desalination unit, only found in study [9]. Several research published on solar flash desalination systems in the literature [2, 3, 4, 6, 11, 14] used a flat plate solar collector as a heat source for flash desalination unit. In this study, we have integrated PTSC with an SSF desalination unit and conducted a numerical study of the system for Basrah city climate. Our current study shows the effect of various parameters on the performance of the SSF desalination process.

2. Case study and process description

In the proposed flash evaporation desalination system, a parabolic trough solar collector powering a single stage flash desalination unit in Basrah city climate, Iraq, as illustrated in Fig. 1. The integrated system comprises two directly coupled sub-systems: the PTSC and the SSF desalination system. The preheated brine water coming from condenser was used as a HTF for PTSC, which gets heated to a specific temperature referred to as the TBT.

A PTSC system is basically consisted of an aluminum parabolic trough shaped surface that serves as a reflector, directing and concentrating direct solar radiation from the sun onto a copper receiver tube with outer diameter 19 mm and 1.25 mm thickness positioned along the focal line of the parabola. The system includes a glass cover with 58 mm inner diameter and 1 mm thickness, an absorber pipe through which HTF passes, and supporting structures. The internal space of the solar receiver tube is filled with a brine water working as an HTF.

The thermal process within a PTSC system relies on the thermal equilibrium between the HTF and its surroundings. The parabolic trough collects solar energy from the sun and directs it towards the solar receiver. Within the solar receiver, the absorber tube absorbs a portion of the reflected energy, thereby elevating the temperature of the HTF. The collected solar energy by PTSC is depend upon the collector area and geometrical profile. The geometrical parameters of solar collectors that are used in the study listed in Table 1.

The remaining energy is transferred back to the outer surface of the receiver through conduction, which then transfers the energy to the internal surface of the glass cover through convection and radiation. The energy is then transferred from the internal surface of the glass cover to the external surface of the glass cover through conduction, and from the external surface to the ambient through convection and radiation, resulting in losses. It is assumed that convection

heat transfer takes place from the solar receiver to the inner wall of the glass cover in the circumferential direction.

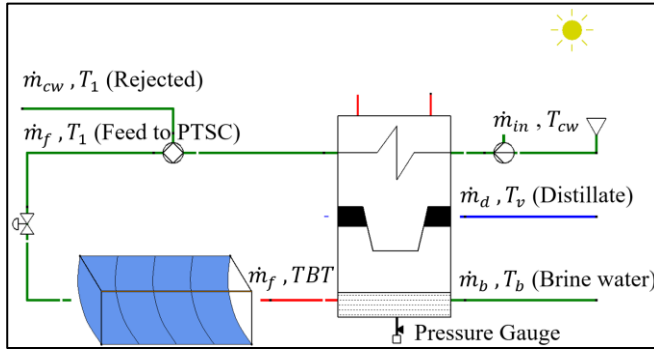


Fig. 1 Schematic of SSF desalination system coupled directly.

The second subsystem is the once-through (OT) SSF desalination unit, which includes a flashing chamber consisting of a brine pool, condenser tubes, demister, and collecting distillate tray. The heated brine water from the PTSC at a flow rate of \dot{m}_f and desired temperature (TBT), flows through the flashing chamber. The flashing chamber is maintained at a certain operating pressure (vacuum pressure), which is lower than the saturation pressure at which the heated saline water enters. The flash chamber coupled with PTSC_6 operates under 10 kPa, 15 kPa and 20 kPa vacuum pressure was investigated. While, the SSF coupled with PTSC_1, PTSC_2, PTSC_3, PTSC_4, and PTSC_5 operates under 40 kPa vacuum pressure and 76.327 C saturation temperature.

During the process of flashing, a portion of the sensible heat present in the brine is converted into latent heat through the evaporation of a small fraction of the brine, \dot{m}_d due to suddenly decrease in the pressure of the brine water. The formation of distillate also leads to an increase in the salinity of the brine from X_f to X_b . The resulting vapor passes through the demister pad and releases its latent heat, $h_{fg,v}$, as it condenses on the tubes of the brine water condenser. The condensed vapor is collected on the distillate tray. The latent heat of condensation is transferred to the incoming brine water, ($\dot{m}_{in} = \dot{m}_{cw} + \dot{m}_f$), and causes its temperature to rise from T_{cw} to T_1 . The cooling water, \dot{m}_{cw} , is discharged, while the feed water, \dot{m}_f , is introduced into the solar collector. The enhancement of overall desalination process efficiency occurs through the recovery of latent heat by the feed water. This decreases the heating required in the solar collector by elevating the feed water temperature from T_1 to TBT instead of T_{cw} to TBT. The remaining brine is rejected at the outlet of the flashing chamber, giving the process its name, the Once-Through SSF desalination system.

Table 1. The geometrical parameters of PTSC.

| PTSC | L (m) | W_a (m) | f (m) | A_{net} (m ²) |
|--------|-------|-----------|---------|-----------------------------|
| PTSC_1 | 6.6 | 2 | 0.5 | 12.408 |
| PTSC_2 | 6 | 1.85 | 0.4625 | 10.434 |
| PTSC_3 | 4.8 | 1.85 | 0.4625 | 8.3472 |
| PTSC_4 | 3.6 | 1.85 | 0.4625 | 6.26 |
| PTSC_5 | 2.4 | 1.85 | 0.4625 | 4.1736 |
| PTSC_6 | 1.7 | 1 | 0.25 | 1.598 |

3. Mathematical and thermal analysis of PTSC and SSF

In PTSC, the concentration of solar radiation is achieved by reflecting the incident solar flux from the concentrator's aperture area (A_a) to the outer receiver area (A_r). The concentration ratio (C), represents the ratio of the aperture area to the receiver area:

$$C = \frac{A_a}{A_r} = \frac{W_a L}{\pi D_{ro} L} \quad (1)$$

The geometrical profile of the parabola in terms of the coordinate can be described as:

$$y^2 = 4fx \quad (2)$$

In the context of a parabola, where f denotes the focal length of the parabola, indicates the position of the receiver and is determined in terms of the aperture width (W_a) by the following formula [19]:

$$f = \frac{W_a}{4 \tan 0.5\phi_r} \quad (3)$$

The concentrator's rim receives the incident radiation beam, and the angle (ϕ_r), formed by the reflected beam radiation and the center line, is referred to as the rim angle. It can be determined by the following expression [20]:

$$\phi_r = \tan^{-1} \left[\frac{8(f/W_a)}{16(f/W_a)^2 - 1} \right] \quad (4)$$

The thermal evaluation of a PTSC involves analyzing the energy balance to determine the portion of incoming radiation that is effectively converted into useful energy for the HTF. To model such systems, several simplifying assumptions are commonly made:

- Thermal performance is assessed under steady-state conditions.
- The thermophysical and optical properties of materials remain constant regardless of temperature.
- Heat losses through support brackets are disregarded.
- The impact of dust and dirt is negligible.

The thermal performance of the PTSC is outlined through basic parameters. It includes the thermal efficiency, the available solar energy, the useful heat gain of the HTF, Q_u , the heat transfer behavior, the friction factor and the corresponding pressure drop. The thermal efficiency (η) of a PTSC can be expressed as the ratio of the useful heat gain of the HTF, (Q_u), to the available solar beam radiation intercepted by the collector aperture area, (Q_s). Mathematically, it is represented as follows [21]:

$$\eta = \frac{Q_u}{Q_s} = \frac{\dot{m}_f c_p (TBT - T_1)}{I_b A_a} \quad (5)$$

Considering a PTSC with an aperture area A_a , the energy balance equation for the cylindrical absorber can be expressed as follows [22]:

$$Q_s = Q_u + Q_L + \frac{dE}{dt} \quad (6)$$

To express (6) in terms of an overall loss coefficient, U_L , the rate of heat loss from the absorber (Q_L) can be written as:

$$Q_L = U_L A_r (T_r - T_{air}) \quad (7)$$

After substituting (7) into (6) and considering steady-state conditions ($dE/dt = 0$), the terms can be rearranged to yield the following equation [23].

$$Q_u = \eta_o I_b A_a - U_L A_r (T_r - T_{air}) \quad (8)$$

The challenge with this equation lies in the calculation or measurement of the average temperature of the absorber surface, T_r . Determining T_r is complex as it depends on various factors such as the collector design, incident solar radiation, and entering fluid conditions. However, an alternative approach is available by utilizing T_{fi} , which represents the inlet fluid temperature, instead of T_r . This can be achieved by introducing a heat removal factor, denoted as F_R [22]:

$$Q_u = F_R [\eta_o I_b A_a - U_L A_r (T_{fi} - T_{air})] \quad (9)$$

$$F_R = \frac{\dot{m} c_p}{A_r U_L} \left[1 - \exp \left(- \frac{A_r U_L F'}{\dot{m} c_p} \right) \right] \quad (10)$$

The heat removal factor holds significant importance as it serves as a crucial design parameter, quantifying the thermal resistance that the absorbed radiation encounters before reaching the HTF. Based on (9), F_R can be defined as the ratio of the useful heat gain of the fluid to the gain that would be obtained if the absorber were uniformly at the temperature T_{fi} . Note that F_R can range from 0 to 1.

The collector efficiency factor, denoted as F' , corresponds to the ratio between the useful heat gained by the fluid and the heat gain that would take place if the entire absorber operated at the local fluid temperature. Mathematically, it can be expressed as follows [22]:

$$F' = \frac{\frac{1}{U_L}}{\frac{1}{U_L} + \frac{D_{ao}}{h_f D_{ai}} + \frac{D_{ao} \ln(D_{ao}/D_{ai})}{2K_a}} \quad (11)$$

Upon dividing (9) by the solar energy intercepted by the collector aperture area, Q_s , the resulting expression is:

$$\eta = \frac{Q_u}{Q_s} = F_R \left[\eta_o - \frac{U_L}{C} \left(\frac{T_{fi} - T_{air}}{I_b} \right) \right] \quad (12)$$

Where η_o is the optical efficiency of the PTSC, representing the ratio of solar energy collected by the absorber to the solar energy intercepted by the concentrator.

The radiation heat transfer by between the absorber and the cover (Q_{loss}) can be calculated from the following equation:

$$Q_{loss} = \frac{\pi D_{ao} L \sigma (T_r^4 - T_c^4)}{\frac{1}{\varepsilon_a} + \frac{(1 - \varepsilon_c) D_{ao}}{\varepsilon_c D_{ci}}} \quad (13)$$

In general, it is important to highlight the significant impact of the concentration ratio on minimizing thermal losses in a PTSC. As shown in (12), a higher concentration ratio directly corresponds to increased efficiency. Moreover, the optical efficiency also plays a decisive role in the overall performance.

The convective heat transfer coefficient of the fluid (h_f) can be expressed as follows:

$$h_f = \frac{Nu_f K_f}{D_{ai}} \quad (14)$$

The Nusselt number varies based on the flow type within the absorber, which can be either laminar or transitional/turbulent. When a fluid circulates in a pipe, laminar flow occurs when $Re_f < 2300$. In this laminar flow regime, the Nusselt number remains unaffected by the Reynolds and Prandtl numbers, taking on a constant value of 4.36 [19]. On the other hand, the flow of the HTF enters the turbulent flow region when $Re_f > 4000$. If $Re_f > 2300$, Nu_f can be determined using the following formula [22]:

$$Nu_f = \frac{f/8 (Re_f - 1000) Pr_f}{1 + 12.7(f/8)^{0.5} (Pr_f^{2/3} - 1)} \quad (15)$$

Equation (15) is applicable for $0.5 \leq Pr_f \leq 2000$ and $2 \times 10^3 < Re_f < 5 \times 10^6$. To estimate the friction factor f , the Colebrook's iterative formula can be used [20]:

$$\frac{1}{\sqrt{f}} = -2 \log \left(\frac{\xi}{3.71 D_{ai}} + \frac{2.51}{Re_f \sqrt{f}} \right) \quad (16)$$

Here, ξ represents the pipe roughness.

The significance of the pressure drops in the collector ΔP lies in its impact on energy consumption, as elevated values of ΔP result in increased energy usage.

$$\Delta P = f \frac{\rho u^2 L}{2 D_{ai}} \quad (17)$$

In formulating the model of SSF analysis, the following assumptions are employed to simplify the analysis procedures:

- The distillate is assumed to be free of salt, a valid assumption given that the boiling point of water is significantly lower than that of salt.
- Specific heat at constant pressure, C_p , equal to 4.18 kJ/kg °C and remains constant for all liquid streams, including brine, distillate, and seawater.
- The overall heat transfer coefficient in the condenser, U_c , is constant and equal to 2 kW/m² °C.
- The system analysis does not include the power requirements for pumps and auxiliaries.
- The heat losses to the surroundings are negligible due to the well-insulated of the flashing stage.

The mathematical model for the single stage flash unit is simple and it includes total mass and salt balances, rate equations for the heat transfer units, as well as energy balances for the solar collector and the condenser [24]. The total mass and salt balances are:

$$\dot{m}_f = \dot{m}_b + \dot{m}_d \quad (18)$$

$$X_f \dot{m}_f = X_b \dot{m}_b \quad (19)$$

Equation (19) assumes that the salt concentration, X_d , in the formed vapor is zero. The solar collector and condenser energy balances are given respectively by;

$$Q_u = \dot{m}_f C_p (TBT - T_1) \quad (20)$$

$$\dot{m}_d h_{fg,v} = \dot{m}_{in} C_p (T_1 - T_{cw}) = \dot{m}_f C_p \Delta T_{st} \quad (21)$$

The heat transfer rate equation for the condenser is;

$$\dot{m}_d h_{fg,v} = U_c A_c (LMTD)_c \quad (22)$$

Where the Logarithmic Mean Temperature Difference $(LMTD)_c$ in the condenser is given in the following;

$$(LMTD)_c = \frac{(T_1 - T_{cw})}{\ln((T_v - T_{cw}) / (T_v - T_1))} \quad (23)$$

The unit thermal performance ratio, defined as the ratio between the required power for evaporating the brine to the total solar power incident on the collector:

$$PR = \frac{\dot{m}_d h_{fg,v}}{\dot{m}_f C_p (TBT - T_1)} \quad (24)$$

The stage temperature drop ΔT_{st} is equal to the difference $(TBT - T_b)$ and is known as the flashing range. On the other hand, the term $(TBT - T_1)$, as is shown in Fig. 2, is equal to the sum of the stage temperature drop ΔT_{st} the stage terminal temperature difference, TTD_c , and the thermodynamic losses.

$$\Delta T_{st} = TBT - T_b \quad (25)$$

$$TBT - T_1 = \Delta T_{st} + \Delta T_{loss} - TTD_c \quad (26)$$

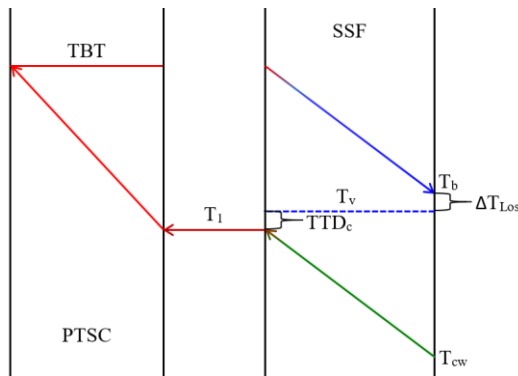


Fig. 2 Temperature Profile for PTSC and SSF desalination system.

The thermodynamic losses (ΔT_{loss}) are the temperature difference of the brine leaving the stage, T_b , and the condensation temperature of the vapor, T_v . In a single stage flashing unit, these losses are caused by the boiling point elevation, the non-equilibrium allowance, and the temperature drop corresponding to the pressure drop during condensation. The terminal temperature difference of the condenser, TTD_c , is equal to temperature difference of the condensing vapor, T_v , and the brine leaving the condenser, T_1 .

4. Validation model of PTSC

The validation of the PTSC model coupled with SSF in EBSILON 16.02 (2022) software was performed by using an experimental result by Dudley et al. [25] about the LS-2 module. Figure 3 displays the validation results that provide high accuracy of the present model. The mean average of the outlet temperature was approximately 1.2%, a value that falls within the range of experimental errors and is relatively low.

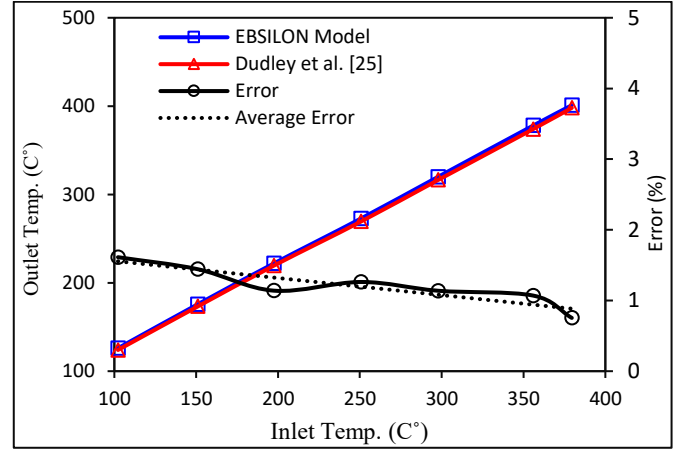


Fig. 3 Validation results compared with Dudley et al. [25].

5. Results and discussion

In this section, single stage flash (SSF) desalination unit integrated with a parabolic trough solar collector (PTSC) was presented, and its performance was numerically analysis. The numerical analysis in this paper was performed depend on Basrah city climate, Iraq by using EBSILON professional 16.02 (2022) software. The results of distillate production, performance ratio and recovery ratio are presented. In addition, the impact of some operational variables on the system's performance are conducted.

As illustrated in Fig. 4, On the first day of June, beam irradiance is available for a 12-hour duration, spanning from 6:00 to 18:00. It is observed that the daily beam irradiance (I_b) rises until noon, reaching its peak value. Subsequently, decreasing in the afternoon due to fluctuations in daily weather conditions. The maximum normal beam irradiance is recorded around 12:00 when solar radiation attains its peak. As indicated in the figure, the useful heat gains proportional increase with beam irradiance available. This is due to the fact that the useful heat gain is strongly influenced by the incident beam radiation and therefore follows its variation.

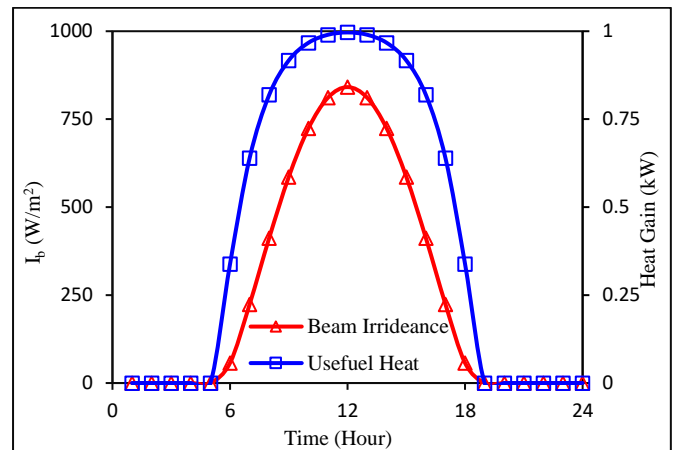


Fig. 4 Beam Irradiance for Basrah City 1st day of June for PTSC-1.

Using EBSILON software, the calculated normal beam irradiance at solar noon stands at 841 W/m^2 . Basrah city annually registers the highest amount of solar radiation during the months of June and July, as illustrated in the Fig. 5.

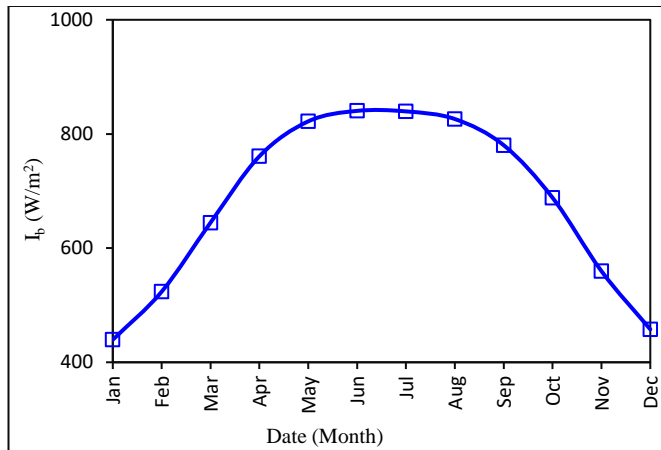


Fig. 5 Annually Beam Irradiance for Basrah City Climate.

Figure 6 showed the measured TBT values exhibit a range from $52.9 \text{ }^\circ\text{C}$ at the beginning of the day to a peak of $107.5 \text{ }^\circ\text{C}$ at 12:00. As solar radiation increases, the TBT value incrementally rises until it reaches its maximum at solar noon. Analysis of the collected environmental data confirms that solar radiation is the primary factor determining the increase in TBT values.

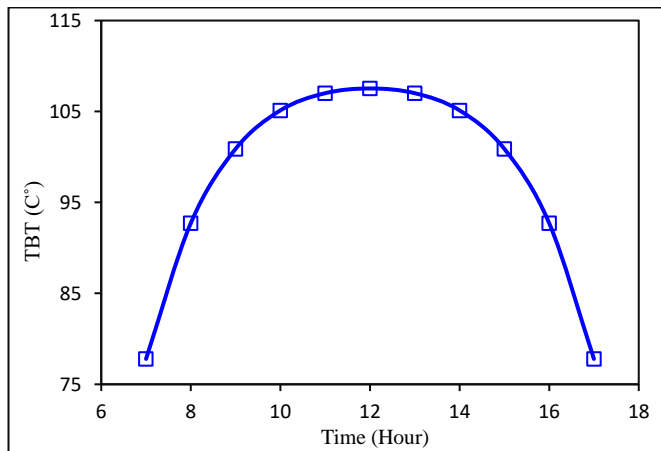


Fig. 6 Effect of Normal Beam Irradiance on TBT with Time in 1st June.

The solar collector heated the brine water coming from condenser depending on available solar radiation absorbed by collector to reach the TBT before entering the flash chamber. Figure 7 illustrates how solar beam radiation influences on TBT values in February and October. In February, the TBT value gradually increases as solar radiation rises. In contrast, throughout October the TBT decreases due to a reduction in solar beam radiation at the same inlet temperature. There is a proportional relation between TBT and distillate water production as shown in the graph. As the TBT increases, the flash range raise resulting an increase in the distillate production and Visca versa.

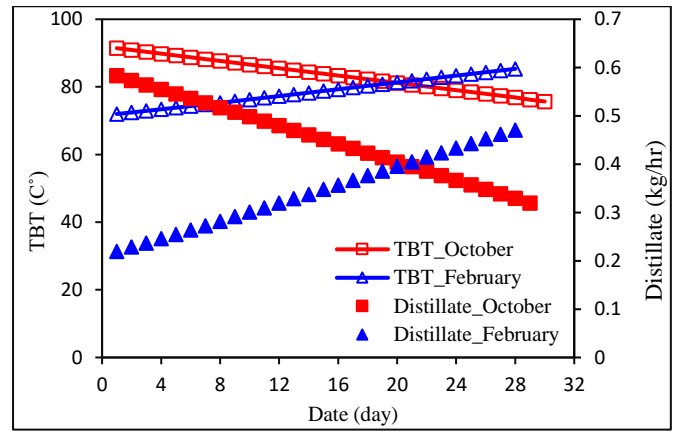


Fig. 7 Effect of Monthly I_b on TBT and Distillate water with Date.

Figure 8 displays the cumulative distillate production rate in 1st June. The total distillate for this day amounted to 7.9 kg, with an average production rate of around 0.7 kg/h . As shown in graph, the distillate increase was linear with time due to rise in TBT resulting from increase of solar radiation for constant feed mass flowrate. The variance in the distillate output is associated to the amount of solar energy absorbed by the system.

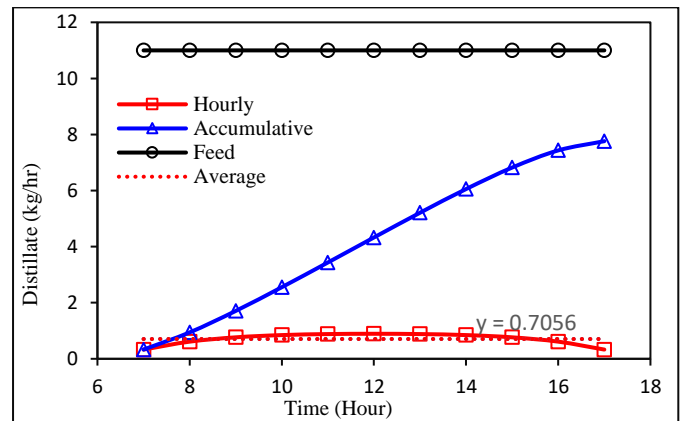


Fig. 8 Effect Normal Beam Irradiance on Distillate water with Time.

Figure 9 displays the annually distillate production and performance ratio. The maximum distillate was 0.895 kg/h at June, with an annual average production of around 0.57 kg/h . It can be observed that when TBT rises from $62.3 \text{ }^\circ\text{C}$ in January to $107 \text{ }^\circ\text{C}$ in June, the PR increases from 0.075 to 0.56 respectively. With a consistent feed water flow rate of 11 kg/h , an elevation in TBT leads to a corresponding increase in distilled water production, consequently raising the PR.

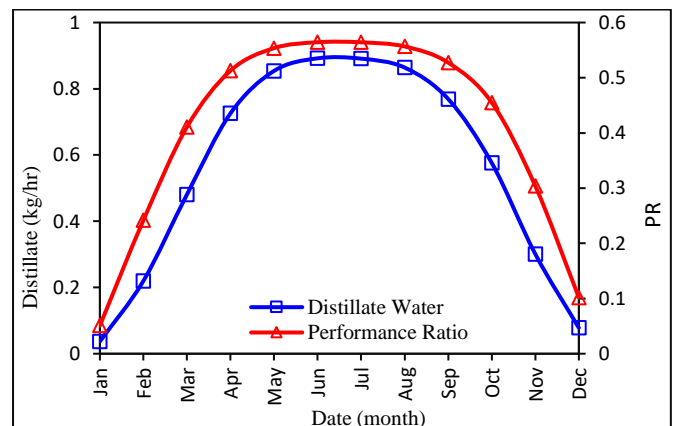


Fig. 9 Annually Effect of I_b on Distillate water & PR.

The impact of vacuum pressure on the desalination process was investigated. In Fig. 10, the distillation rates of a solar distillation system are illustrated under various vacuum pressures. At vacuum pressures of 20, 15, and 10 kPa, the measured distillation rates were 0.7, 0.818, and 0.968 kg/h, respectively. The brine flow rate was set to 11 kg/h for this case. The operational duration for each vacuum pressure maintained from 6:00 to 18:00 on the 1st June to ensure performance of the solar thermal collectors at same day.

The daily distillate per unit area of solar collector plays a crucial role in performance analysis, serving as a key indicator of the solar desalination unit's efficiency. Figure 11 demonstrates the daily productivity associated with each operating vacuum pressure. As expected, reducing the pressure within the chamber of the SSF system resulted in improved distillation rates. The solar SSF system's productivity per solar collector unit area at 20 kPa, 15 kPa, and 10 kPa vacuum pressures was 4.7 kg/day/m², 5.3 kg/day/m², and 6.25 kg/day/m², respectively. The distillate production at vacuum pressures of 10 kPa and 15 kPa is 37% and 16% higher than that at 20 kPa, respectively.

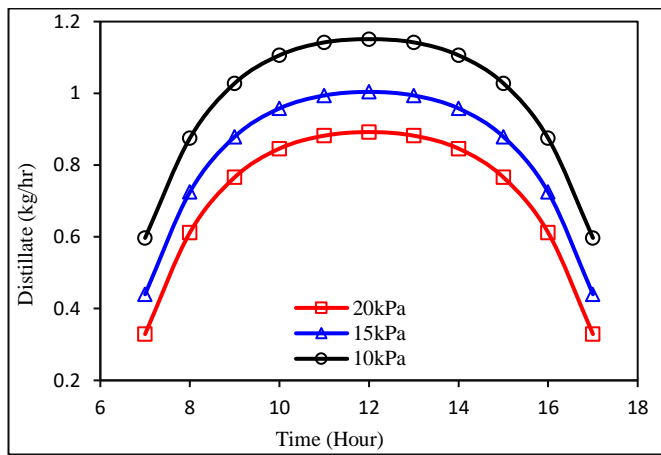


Fig. 10 Effect Vacuum pressure on Distillate production with Time.

The driving force for vapor flashing is the pressure difference between the brine water in and out of the chamber. The reduction in vacuum pressure minimizes the required of thermal energy input, thereby contributing energy savings.

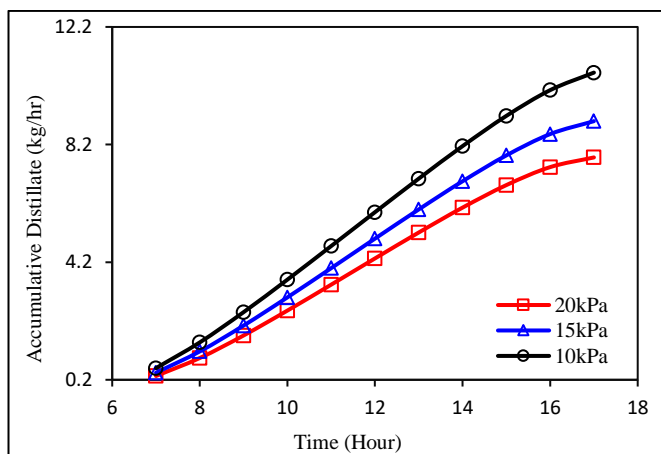


Fig. 11 Effect Vacuum pressure on cumulative Distillate with Time.

Figure 12 illustrates the impact of varying TBT on the daily distillate output of the desalination system. With the rise of the TBT, there is a corresponding elevation in the energy input to

the chamber, leading to an increase in the output of distillate water and then rises of daily distillate production. At vacuum pressures of 20, 15, and 10 kPa, the average daily distillation rates were 7.8, 8.99, and 10.65 kg/day, respectively. With consider that TBT rises until noon, reaching its peak value. Subsequently, decreasing in the afternoon due to fluctuations in daily weather conditions under the effect the normal beam irradiance.

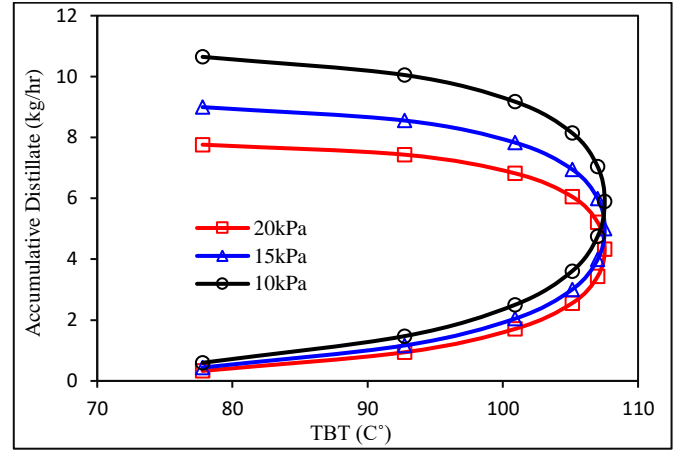


Fig. 12 Effect Vacuum pressure on cumulative Distillate with TBT.

Figure 13 illustrates the impact of varying TBT on the distillate water output of the desalination system. Clearly, as the TBT rises, there is a corresponding increase in the energy input to the stage, resulting in higher distillate water output. As the TBT is reached to 107 °C in solar noon, the distillate water output rise to 0.9 kg/h with a constant feed mass flowrate of 11 kg/h. The average daily distillate production is observed to be 7.8 kg/day, and this is achieved with solar collector area of 1.7 m². This can be represented as 4.7 kg/m²/day under 20 kPa vacuum pressure.

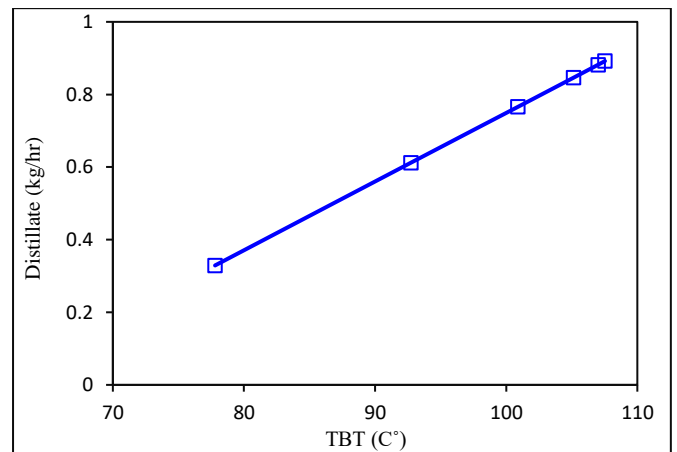


Fig. 13 Effect TBT on Distillate Production.

Figure 14 shows the impact of varying vacuum pressure with different TBT on the distillate water production of the desalination system. Clearly, as vacuum pressure decreases, the boiling point of brine water decreases, there is a corresponding increase in the flashing range of the stage, resulting in higher distillate water output. As the TBT is increased, the distillate water output rise for each vacuum pressure due to increase temperature difference inside chamber.

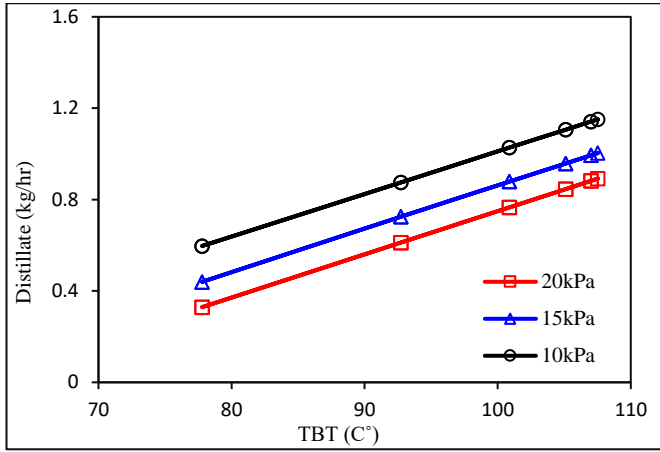


Fig. 14 Effect Vacuum pressure on Distillate production with TBT.

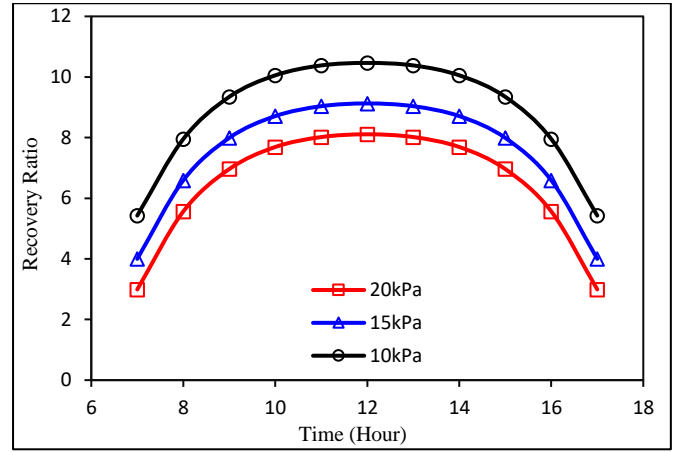


Fig. 16 Effect Vacuum pressure on Recovery Ratio with Time.

The recovery ratio (RR), illustrated in Fig. 15, represents the ratio of distillate mass flowrate to brine feed water mass flowrate. This ratio rises with an increase in TBT, indicating a primary dependence on TBT. For each TBT value, there exists a consistent distillate amount that results in a stable recovery ratio at specified vacuum pressure. The maximum observed values are around 8.1%, 9.12% and 10.46% at 107°C for vacuum pressure 20 kPa, 15 kPa and 10 kPa respectively, indicating that 100 kg of feedwater is needed to yield 10.46 kg at 10 kPa vacuum pressure of distillate as example. These values are considered acceptable for a single-stage system.

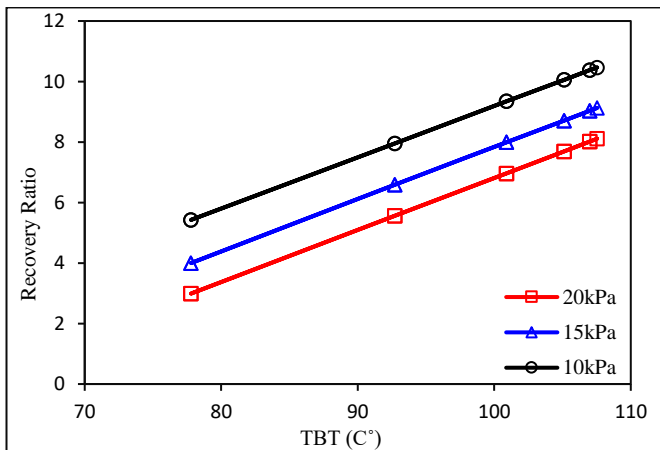


Fig. 15 Effect Vacuum pressure on Recovery Ratio with TBT.

Figure 16 illustrates how the recovery ratio of the desalination system changes with time under various vacuum pressures. As solar radiation increases resulting an increase TBT, the RR value incrementally rises until it reaches its maximum at solar noon. The fluctuations in RR for different vacuum pressures during the solar day align with the availability of solar energy.

Figure 17 illustrates how the recovery ratio of the desalination system changes annually under 20 kPa vacuum pressures for constant feed brine water. The recovery ratio proportional with the availability of solar energy, as solar radiation increases then the RR value incrementally rises until it reaches its maximum in June. This raise of RR depends on distillate water increasing due to increases TBT, the average annually RR was 5% for constant feed brine water.

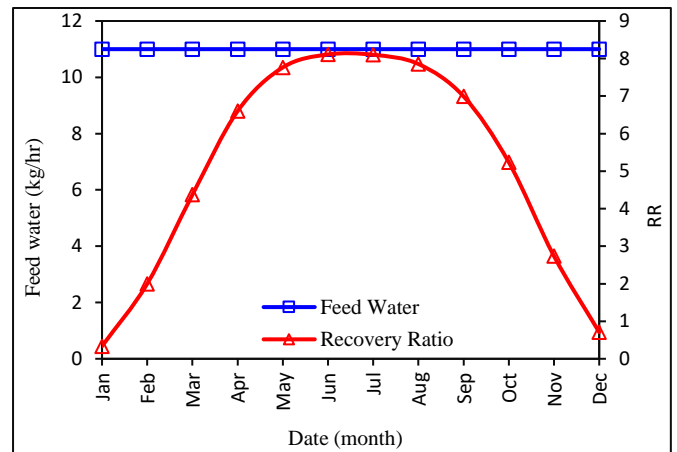


Fig. 17 Effect I_b on Recovery Ratio at Const. Feed with Date.

Figure 18 illustrates the impact of the TBT on the performance ratio (PR) of the desalination system at 10 kPa, 15 kPa and 20 kPa vacuum pressures. The graph demonstrates a direct proportionality between the change in PR and TBT. When the TBT is higher, less energy is required to convert the brine feed water into vapor. Consequently, an improvement in performance ratio occurs as less heat is necessary to produce the same amount of vapor. Furthermore, as the TBT increases for a constant brine feed water flow rate of 11 kg/h, the amount of distilled water also increases, causing a rise in PR. It can be observed that when TBT rises from 77°C to 107°C, the PR increases from 0.32 to 0.56, 0.43 to 0.63 and 0.59 to 0.73 for 20 kPa, 15 kPa and 10 kPa respectively.

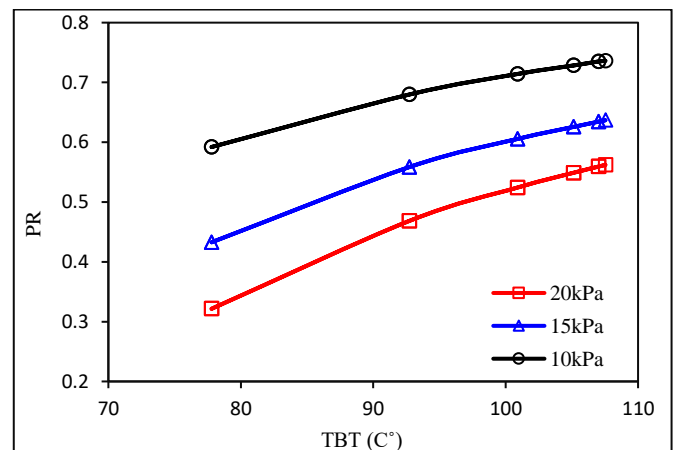


Fig. 18 Effect Vacuum pressure on Performance Ratio with TBT.

Figure 19 illustrates how the daily performance ratio (PR) at vacuum pressures of 10 kPa, 15 kPa, and 20 kPa is influenced by solar radiation availability with time. The average PR values are determined to be 0.694, 0.577, and 0.491 for 10 kPa, 15 kPa, and 20 kPa, respectively. The performance ratio is shown to be sensitive to factors such as solar availability.

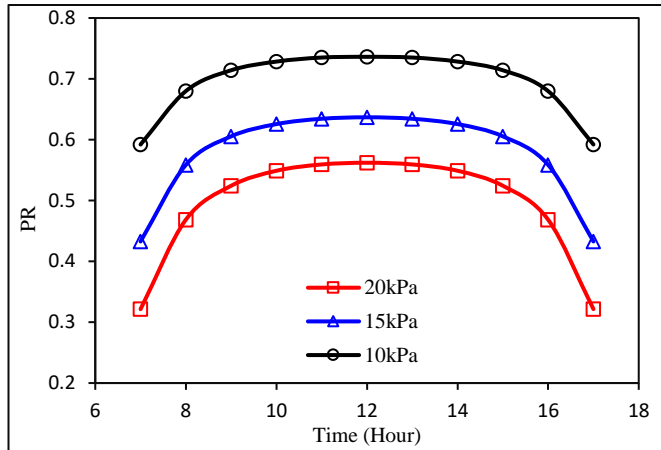


Fig. 19 Effect Vacuum pressure on Performance Ratio with Time.

An analysis of the daily solar beam radiations, HTF temperature difference and collector efficiency from 9:00 to 15:00 was carried out and shown in Fig. 20. The daily collector efficiency decreases gradually with time until reaching its minimum value at solar noon. Despite the rise in temperature difference due to an increase in solar radiation, the rate of increase in solar radiation is higher than that of augmentation in temperature difference when the feed brine water remains constant. Consequently, the collector efficiency decreases over time as solar radiation increases.

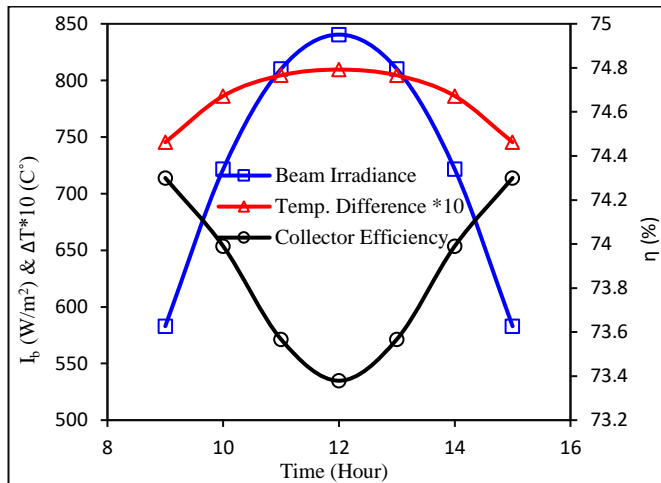


Fig. 20 Daily Collector Efficiency, Temperature Difference and I_b .

Figure 21 illustrates that the annually collector efficiency rises with solar radiation. Although feed brine water is constant, the TBT raise due to increase of solar radiation. The rate of increase in TBT is higher than that of augmentation in solar radiation at any given time, hence the collector efficiency is enhanced eventually as TBT increases.

The analysis of the collector pressure drops, as illustrated in Fig. 22, is conducted. This understanding is crucial, particularly when operating with a low brine feed water. Initially, during the morning, the collector pressure drop is

important due to the fact that the HTF is more viscous, thereby increasing the friction between the fluid and the absorber walls. Until reach solar noon, the pressure drop undergoes a characteristic shrinking due to the HTF absorbing more heat, expanding thermally, and consequently becoming less dense. This results in a reduction of the frictional forces contributing to the pressure drop in the absorber. The fluid properties are more dominant on pressure drop than mass flowrate of feed brine water in this case. The highlight point is the amount of solar energy absorbed by collector and what does it depend on.

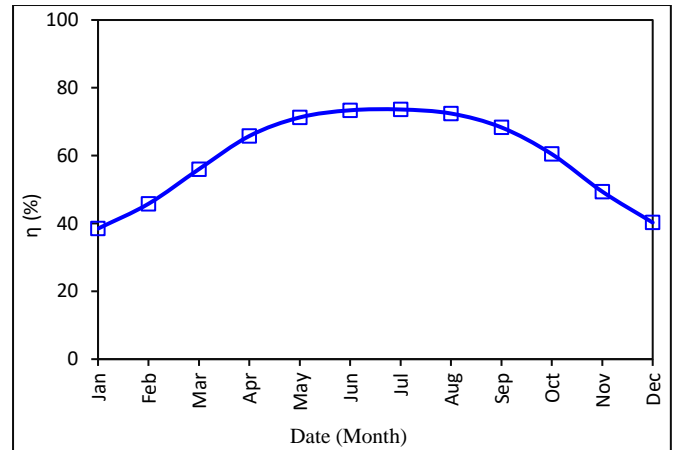


Fig. 21 Annually Collector Efficiency.

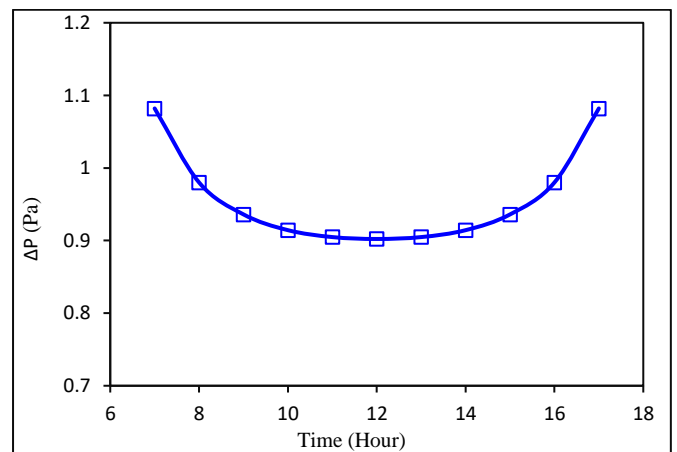


Fig. 22 Effect of Solar radiation on Pressure Drop with Time.

Figure 23 illustrates the variations in solar energy absorption across five different collector areas on a specific date. As expected, an increase in collector area led to a corresponding rise in the absorbed solar energy, contingent upon the availability of solar radiation. The maximum and minimum solar energy absorbed occurred at collector areas of 12.408 m² (PTSC_1) and 4.1736 m² (PTSC_5), registering 3.55 kW and 1.19 kW in January, and 7.82 kW and 2.63 kW in June, respectively.

The PTSC heated the feed brine water which is coming from condenser at T_1 to reach the desired temperature (TBT) before entering flash chamber. Because solar radiation varies depending on the date and time, the feed brine water must be adjustable to maintain a constant TBT. When the feed brine water is increased to achieve a TBT of 107°C, these adjustments result in an increase in the collector pressure drop, as illustrated in Fig. 24. This figure shows the effect of brine feed water on pressure drop for different collector area. Increasing the feed brine water results in an increased velocity,

leading to higher pressure drop due to gain in kinetic energy. Additionally, the Reynolds number may increase, leading to changes in the friction factor and subsequently increasing the pressure drop.

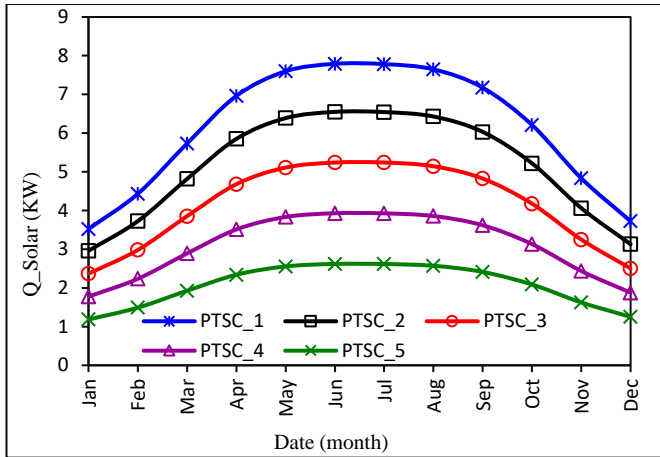


Fig. 23 Effect of Collector area on Solar Energy Absorbed with Date.

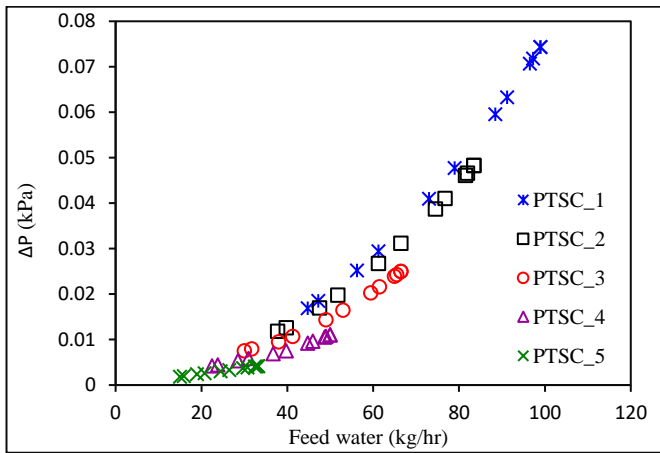


Fig. 24 Effect of Feed Brine Water on Pressure Drop for Different Collector Length.

Figure 25 illustrates the effect of raise feed brine water across five different collector areas on a distillate production. Increasing the mass flow rate of feed brine water led to higher distillate production, due to an increase the amount of brine feed water that flashes into vapor inside flash chamber under 40 kPa vacuum pressure.

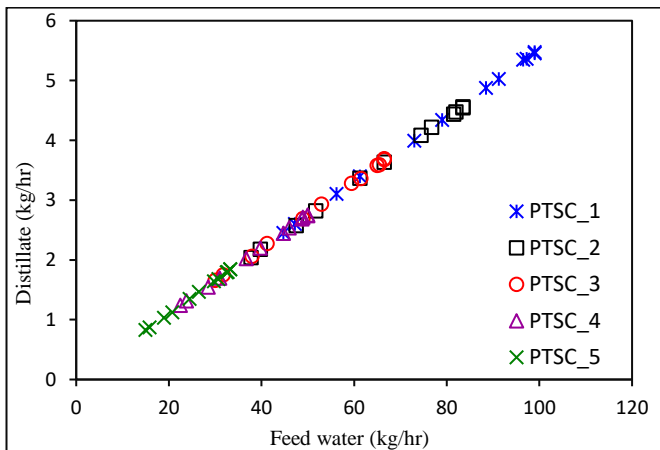


Fig. 25 Effect Feed Brine Water on Distillate Production.

The distillate water production also depends on solar irradiance, as illustrated in Fig. 26 for five different collector area. The maximum observed values in June are around 5.5, 4.56, 3.69, 2.75 and 1.85 kg/h for PTSC_1, PTSC_2, PTSC_3, PTSC_4, and PTSC_5 respectively, when TBT of 107 °C and vacuum pressure 40 kPa. While the average distillate water production reach 4.28, 3.57, 2.88, 2.16 and 1.44 kg/h, respectively. These raises of feed brine water can impact the efficiency of the PTSC.

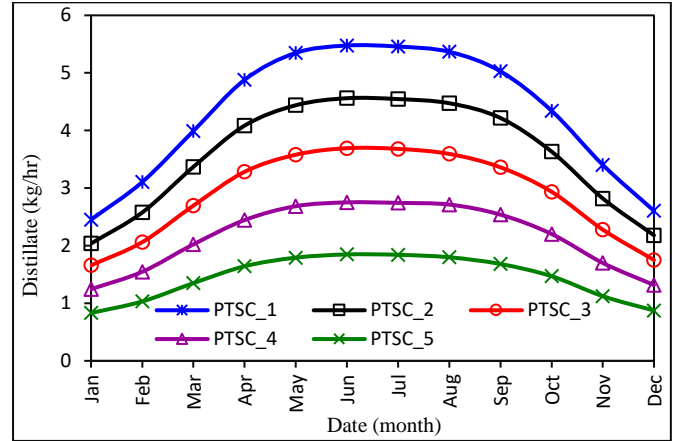


Fig. 26 Effect Solar Irradiance on Distillate Production with Date.

A more efficient solar collector absorbed more solar beam irradiance, requiring a higher mass flowrate to transfer this energy to the feed brine water for constant TBT. As shown in Fig. 27 which illustrated the impact of mass flowrate on collector efficiency.

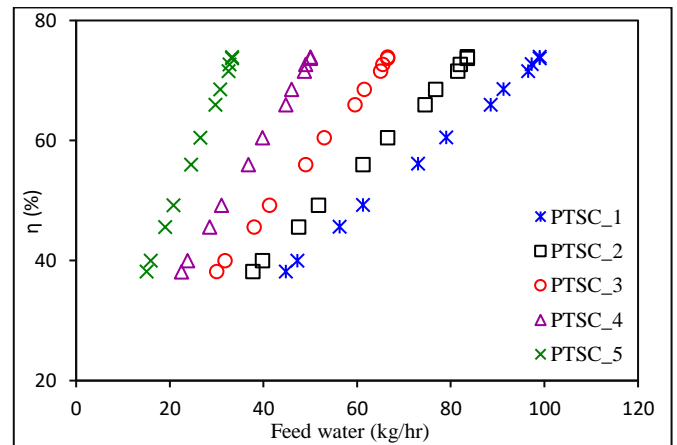


Fig. 27 Effect Feed Brine Water on Collector Efficiency.

Figure 28 illustrates how the recovery ratio of the desalination system affected annually under 40 kPa vacuum pressures for five collectors at constant TBT. Obviously, the recovery ratio is primarily influenced by the mass flow rate rather than the collector area or the amount of solar energy absorbed. The raise of feed brine water corresponding an increase of distillate water. Hence, the solar irradiance has little impact on recovery ratio, the annually average of recovery ratio was 5.5 %.

Figure 29 illustrates how the annually performance ratio (PR) at vacuum pressure of 40 kPa is influenced depend on solar availability date. The average PR value was determined to be 0.43 for different collector area. The performance ratio is shown to be not affected to solar availability and the solar collector area, as much as the number of stages at constant TBT as referred in the previous literature.

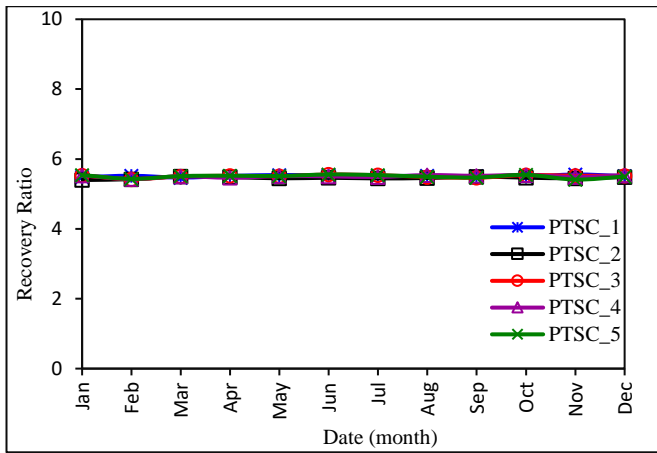


Fig. 28 Annually Recovery Ratio for Different Collector Area.

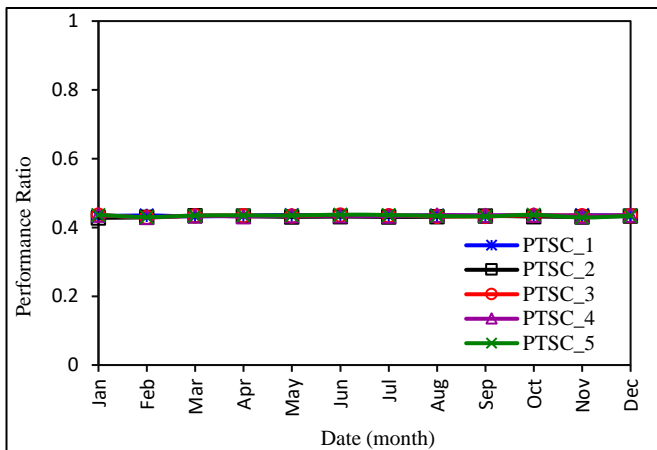


Fig. 29 Annually Performance Ratio for Different Collector Area.

6. Conclusions

In this study, the performance of a new single stage flash desalination system powered by the parabolic trough solar collector is investigated in Basrah city, Iraq based on numerical and theoretical analysis. The numerical simulations were performed via EBSILON professional 16.02 (2022) software. The effects of Top Brine Temperature (TBT), mass flowrate of feed brine water to get the desired TBT, seasonal variations in solar irradiance availability, solar collector area, and vacuum pressure inside flash chamber on the performance of the desalination system was studied. The basic findings of the current study can be summarized as follows:

1. Basrah city annually registers the highest amount of solar radiation during the months of June and July.
2. The proposed system is applicable in Basrah city when compared the results with literature.
3. Analysis of the collected environmental data confirms that solar radiation is the primary factor determining the increase in TBT values, the TBT value gradually increases as solar radiation rises.
4. An elevation in TBT leads to a corresponding increase in distilled water production, consequently raising the performance ratio. The PR is shown to be sensitive to factors such as solar availability.
5. The collector efficiency is enhanced eventually as TBT increases.
6. An increase in the collector pressure drops, when the feed brine water is increased.
7. The daily distillate per unit area of solar collector plays a

crucial role in performance analysis, serving as a key indicator of the solar desalination unit's efficiency.

8. The driving force for vapor flashing is the pressure difference between the brine water in and out of the chamber.
9. As vacuum pressure decreases, the boiling point of brine water decreases, there is a corresponding increase in the flashing range of the stage, resulting in higher distillate water output.
10. The recovery ratio proportional with the availability of solar energy, as solar radiation increases then the RR value incrementally rises.

The current investigation focuses on numerical analysis. Subsequently, the results of the numerical model will undergo comparison with an experimental work in future research. A current study can be extended upon interest in several directions. An optimization simulation to identify the optimal performance, thermo-economic feasibility study may be conducted to demonstrate the net advantages of the proposed model and MSF desalination evaporation system. These recommendations are made for future research.

References

- [1] M. A. Darwish, S. G. Serageldin, and H. T. Eldessouky, "Flashing in desalination units," *Desalination*, vol. 19, no. 1, pp. 93-101, 1976. [https://doi.org/10.1016/S0011-9164\(00\)88020-0](https://doi.org/10.1016/S0011-9164(00)88020-0)
- [2] M. Farwati, "Theoretical study of multi-stage flash distillation using solar energy," *Energy*, vol. 22, no. 1, pp. 1-5, 1997. [https://doi.org/10.1016/S0360-5442\(96\)00056-4](https://doi.org/10.1016/S0360-5442(96)00056-4)
- [3] J. Joseph, R. Saravanan, and S. Renganarayanan, "Studies on a single-stage solar desalination system for domestic applications," *Desalination*, vol. 173, no. 1, pp. 77-82, 2005. <https://doi.org/10.1016/j.desal.2004.06.210>
- [4] A. S. Nafey, M. A. Mohamad, S. O. El-Helaby, and M. A. Sharaf, "Theoretical and experimental study of a small unit for solar desalination using flashing process," *Energy Conversion and Management*, vol. 48, no. 2, pp. 528-538, 2007. <https://doi.org/10.1016/j.enconman.2006.06.010>
- [5] S. C. Maroo, and D. Y. Goswami, "Theoretical analysis of a single-stage and two-stage solar driven flash desalination system based on passive vacuum generation," *Desalination*, vol. 249, no. 2, pp. 635-646, 2009. <https://doi.org/10.1016/j.desal.2008.12.055>
- [6] K. S. Reddy, K. R. Kumar, T. S. O'Donovan, and T. K. Mallick, "Performance analysis of an evacuated multi-stage solar water desalination system," *Desalination*, vol. 288, pp. 80-92, 2012. <https://doi.org/10.1016/j.desal.2011.12.016>
- [7] M. Al-Hamahmy, H. E. S. Fath, and K. Khanafer, "Techno-economical simulation and study of a novel MSF desalination process," *Desalination*, vol. 386, pp. 1-12, 2016. <https://doi.org/10.1016/j.desal.2016.02.018>
- [8] Y. Roy, G. P. Thiel, M. A. Antar, and J. H. Lienhard, "The effect of increased top brine temperature on the performance and design of OT-MSF using a case study," *Desalination*, vol. 412, pp. 32-38, 2017. <https://doi.org/10.1016/j.desal.2017.02.015>
- [9] M. Alsehli, J.-K. Choi, and M. Aljuhan, "A novel design for a solar powered multistage flash desalination," *Solar Energy*, vol. 153, pp. 348-359, 2017. <https://doi.org/10.1016/j.solener.2017.05.082>

- [10] K. Garg, V. Khullar, S. K. Das, and H. Tyagi, "Performance evaluation of a brine-recirculation multistage flash desalination system coupled with nanofluid-based direct absorption solar collector," *Renewable Energy*, vol. 122, pp. 140-151, 2018. <https://doi.org/10.1016/j.renene.2018.01.050>
- [11] I. Darawsheh, M. D. Islam, and F. Banat, "Experimental characterization of a solar powered MSF desalination process performance," *Thermal Science and Engineering Progress*, vol. 10, pp. 154-162, 2019. <https://doi.org/10.1016/j.tsep.2019.01.018>
- [12] M. Alsheekh, S. E. Najim, and H. S. Sultan, "Experimental, Theoretical and CFD Validations for Solar Powered Atmospheric Water Generation Using Thermoelectric Technics," *Basrah journal for engineering science*, vol. 21, no. 2, pp. 17-28, 2021. <https://doi.org/10.33971/bjes.21.2.4>
- [13] H. Jassim Jaber, Q. A. Rishak, and Q. A. Abed, "Using PCM, an Experimental Study on Solar Stills Coupled with and without a Parabolic Trough Solar Collector," *Basrah journal for engineering science*, vol. 21, no. 2, pp. 45-52, 2021. <https://doi.org/10.33971/bjes.21.2.7>
- [14] M. Alsehli, "Experimental Validation of a Solar Powered Multistage Flash Desalination Unit with Alternate Storage Tanks," *Water*, vol. 13, no. 16, 2021. <https://doi.org/10.3390/w13162143>
- [15] A. Babaebazaz, S. Gorjian, and M. Amidpour, "Integration of a Solar Parabolic Dish Collector with a Small-Scale Multi-Stage Flash Desalination Unit: Experimental Evaluation, Exergy and Economic Analyses," *Sustainability*, vol. 13, no. 20, 2021. <https://doi.org/10.3390/su132011295>
- [16] A. K. Thakur, R. Sathyamurthy, R. Velraj, I. Lynch, R. Saidur, A. K. Pandey, S. W. Sharshir, Z. Ma, P. GaneshKumar, and A. E. Kabeel, "Sea-water desalination using a desalting unit integrated with a parabolic trough collector and activated carbon pellets as energy storage medium," *Desalination*, vol. 516, 2021. <https://doi.org/10.1016/j.desal.2021.115217>
- [17] F. Farhadi, M. Deymi-Dashtebayaz, and E. Tayyeban, "Studying a Multi-Stage Flash Brine Recirculation (MSF-BR) System Based on Energy, Exergy and Exergoeconomic Analysis," *Water*, vol. 14, no. 19, 2022. <https://doi.org/10.3390/w14193108>
- [18] Q. Thabit, A. Nassour, and M. Nelles, "Water Desalination Using the Once-through Multi-Stage Flash Concept: Design and Modeling," *Materials (Basel)*, vol. 15, no. 17, Sep 3, 2022. <https://doi.org/10.3390/ma15176131>
- [19] J. Duffie, and W. J. D. Beckman, William A. Beckman, Wiley: *Solar Engineering of Thermal Processes*, John A. 2013.
- [20] S. A. Kalogirou, *Solar energy engineering: processes and systems*: Academic Press 1st Edition, 2013. ISBN 978-0-12-374501-9
- [21] E. Bellos, C. Tzivanidis, K. A. Antonopoulos, and I. Daniil, "The use of gas working fluids in parabolic trough collectors – An energetic and exergetic analysis," *Applied Thermal Engineering*, vol. 109, pp. 1-14, 2016. <https://doi.org/10.1016/j.applthermaleng.2016.08.043>
- [22] G. Coccia, G. D. Nicola, and A. Hidalgo, *Parabolic Trough Collector Prototypes for Low-Temperature Process Heat* (Springer Briefs in Applied Sciences and Technology). 2016. <https://doi.org/10.1007/978-3-319-27084-5>
- [23] G. W. Treadwell, *Design considerations for parabolic-cylindrical solar collectors*, Sandia National Lab. (SNL-NM), Albuquerque, NM (United States), 1976.
- [24] H. El-Dessouky, H. I. Shaban, and H. Al-Ramadan, "Multi-stage flash desalination process: A thermal analysis," *Developments in Chemical Engineering Mineral Processing*, vol. 4, no. 1-2, pp. 5-22, 1996. <https://doi.org/10.1002/apj.5500040102>
- [25] V. Dudley, G. Kolb, M. Sloan, and D. Kearney, "SEGS LS2 solar collector test results, Report of Sandia National Laboratories," SANDIA94-1884, USA, 1994. <https://doi.org/10.2172/70756>

| Nomenclature | | |
|-----------------|---|----------------------------------|
| Symbol | Description | SI Units |
| \dot{m} | Mass flow rate | kg/h |
| X | Salinity | ppm |
| T | Temperature | K |
| W_a | Aperture width | m |
| I_b | Beam irradiance | w/m ² |
| D | Diameter | mm |
| L | Collector length | cm |
| u | HTF velocity | m/s |
| K_a | Thermal conductivity of the absorber | - |
| K_f | Thermal conductivity of the HTF | - |
| Greek Symbols | | |
| Symbol | Description | SI Unit |
| ρ | Density of HTF | kg/m ³ |
| σ | Stefan-Boltzmann constant 5.67×10^{-8} | Wm ⁻² K ⁻⁴ |
| ε_a | Emissivity of the absorber | - |
| ε_c | Emissivity of the cover | - |
| Subscripts | | |
| f | Feed | |
| d | Distillate | |
| cw | Colling water | |
| b | Brine | |
| c | Glass cover | |
| i | Inlet to PTSC | |
| ai | Inner absorber | |
| ao | Outer absorber | |
| ci | Inner glass cover | |
| co | Outer glass cover | |